Article

Electrogenerated Chemiluminescence of a Spirobifluorene-Linked Bisanthracene: A Possible Simultaneous, Two-Electron Transfer

Matthew M. Sartin, Chingfong Shu, and Allen J. Bard

J. Am. Chem. Soc., **2008**, 130 (15), 5354-5360 • DOI: 10.1021/ja8000858 • Publication Date (Web): 13 March 2008

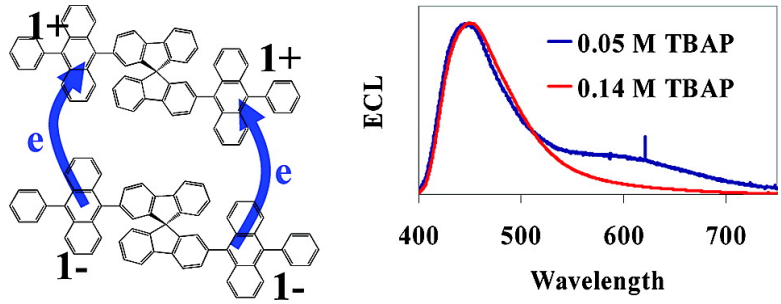

More About This Article

Additional resources and features associated with this article are available within the HTML version:

- Supporting Information
- Links to the 2 articles that cite this article, as of the time of this article download
- Access to high resolution figures
- Links to articles and content related to this article
- Copyright permission to reproduce figures and/or text from this article

View the Full Text HTML

J|A|C|S
ARTICLES

Published on Web 03/13/2008

Electrogenerated Chemiluminescence of a Spirobifluorene-Linked Bisanthracene: A Possible Simultaneous, Two-Electron Transfer

Matthew M. Sartin,[†] Chingfong Shu,[‡] and Allen J. Bard*,[†]

Chemistry and Biochemistry Department, The University of Texas at Austin, Austin, Texas 78712, and Department of Applied Chemistry and Microelectronics and Information Systems Research Center, National Chiao Tung University, Hsin-Chu, Taiwan 300, Republic of China

Received January 4, 2008; E-mail: ajbard@mail.utexas.edu

Abstract: We report the electrogenerated chemiluminescence (ECL) of 2,2′-bis(10-phenylanthracen-9-yl)-9,9′-spirobifluorene (spiro-FPA), a dichromophoric molecule composed of two phenylanthracenes linked by a spirobifluorene moiety (PA∼X∼PA). The results are compared to those for 9,10-diphenylanthracene (DPA), a related molecule with a single chromophore. Cyclic voltammetry (CV) of spiro-FPA shows two reversible, closely spaced, one-electron transfers on both reduction and oxidation, occurring at $E^{\circ}_{1,red} = -2.02$, $E^{\circ}_{2,red} = -2.07$ V vs SCE and $E^{\circ}_{1,ox} = 1.14$, $E^{\circ}_{2,ox} = 1.20$ V vs SCE. The potentials for each pair are close enough to appear as a single peak in CV, indicating that the spirobifluorene moiety interrupts conjugation between the redox centers. The potentials observed are similar to those of DPA, which shows $E^{\circ}_{red} = -2.06$ V vs SCE and $E^{\circ}_{ox} = 1.15$ V vs SCE. The absorbance spectrum of spiro-FPA shows $\lambda_{max,abs} = 377$ nm, with $\epsilon_{377} = 25\,700$ M^{-1} s^{-1}, while DPA exhibited $\lambda_{max,abs} = 374$ nm, with $\epsilon_{374} = 13\,800$ M^{-1} s^{-1}, demonstrating that spiro-FPA has twice the available chromophores as DPA. Photoluminescence (PL) data for spiro-FPA shows $\lambda_{max,PL} = 434$ nm, with $\Phi_{PL} = 0.74$, while DPA fluoresces at 420 nm with $\Phi_{PL} = 0.91$; thus, there is greater solvent or structural relaxation in the spiro-FPA excited state, which may account for the greater internal conversion. Unlike DPA, the ECL spectrum of spiro-FPA exhibits long-wavelength emission not observed in the PL. We attribute this emission to excimers formed during annihilation ECL. Steric hindrance prevents DPA from forming excimers, even in ECL, but spiro-FPA annihilation can occur between pairs of di-ions ($PA^{\bullet-}$∼X∼$PA^{\bullet-}$ and $PA^{\bullet+}$∼X∼$PA^{\bullet+}$), which are electrostatically more strongly attracted to one another than the mono-ions. This greater electrostatic attraction may be sufficient to overcome the steric hindrance to excimer formation. Lowering the electrolyte concentration decreases the electrostatic shielding of the ions from one another; thus, the increase in longer wavelength ECL accompanying a decrease in electrolyte concentration supports the role of the di-ions in excimer formation. Additionally, simulations show, consistent with experiment, a more rapid decrease in excimer concentration than in excited monomer concentration as a function of time after each potential pulse. This is probably due to the greater number of scavenging reactions available for di-ions. The simulations are confirmed experimentally when lower potential pulsing frequencies yield lower relative excimer emission. Since an excited state created by one-electron transfer between two di-ions should be rapidly quenched via electron transfer by the other PA moiety, the existence of excimers suggests the possibility of simultaneous, two-electron transfer to generate the excimer.

Introduction

The electrogenerated chemiluminescence (ECL) of 2,2′-bis(10-phenylanthracen-9-yl)-9,9′-spirobifluorene (spiro-FPA, Figure 1) raises the interesting possibility of an outer-sphere, simultaneous, two-electron transfer during the annihilation of the radical di-ion pairs. The electrochemical literature generally favors one-electron, outer-sphere reactions and the concept that apparent two-electron transfers actually consist of two, one-electron transfers separated by a conformational or chemical change in the substrate compound. The determination of the individual redox potentials for these reactions reinforces this view.[1] However, despite the ubiquity of the one-electron transfer mechanism, simultaneous, two-electron transfer has never been proven impossible and has even been suggested in the past.[2,3] In this paper, we show how the formation of excimers during the ECL of spiro-FPA provides some evidence for simultaneous, two-electron transfer during the annihilation between its dianion and dication.

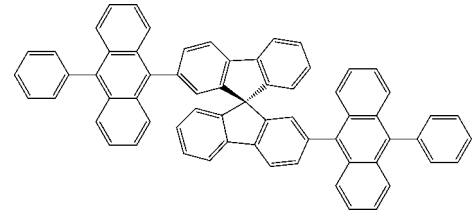

Figure 1. Structure of spiro-FPA.

[†] The University of Texas at Austin.
[‡] National Chiao Tung University.

10.1021/ja8000858 CCC: $40.75

Spiro-FPA consists of two phenylanthracene redox centers (PA) linked by a spirobifluorene unit (PA∼X∼PA). The sp^3 carbon of the spirobifluorene disrupts conjugation between the PA centers. The structure of each redox center is thus analogous to that of 9,10-diphenylanthracene (DPA), a highly luminescent, blue emitter ($\Phi_{PL} \approx 0.91$,[4] $\Phi_{ECL} \approx 0.014$[5]) with stable radical ions[6] and one of the first molecules from which ECL was observed.[7] The structural similarities between spiro-FPA and DPA lead to many similarities in the spectroscopy and electrochemistry of the two molecules. However, two notable differences are electroluminescence, where the greater structural rigidity and steric bulk improve spiro-FPA device stability over that of DPA,[8] and ECL, where the spirobifluorene linkage of two DPA centers encourages excimer formation, despite the additional steric bulk, as discussed below.

ECL is the production of light by the annihilation of electrochemically generated radical ions.[7,9] If ΔH°_{ann}, the enthalpy of radical ion annihilation, exceeds the energy of the first excited singlet state, E_s, the annihilation can directly populate the singlet state (i.e., the system is energy sufficient), as shown in Scheme 1. This is called S-route ECL.

Scheme 1

$$R + e \rightarrow R^{\bullet -} \quad (1)$$

$$R - e \rightarrow R^{\bullet +} \quad (2)$$

$$R^{\bullet +} + R^{\bullet -} \rightarrow {}^1R^* + R \quad (3)$$

$${}^1R^* \rightarrow R + h\nu \quad (4)$$

If a co-reactant is used, only one of the radical ions is necessary to generate ECL. For example, the co-reactant persulfate can be electrochemically reduced to generate the powerful oxidizing agent, $SO_4^{\bullet -}$, as shown in Scheme 2. $SO_4^{\bullet -}$ can then oxidize the anion radical formed in the same potential step without directly generating the cation radical at the electrode surface. Co-reactant ECL is used when annihilation is difficult to achieve due to a narrow solvent window or rapid homogeneous reactions of one of the radical ions. Because co-reactants largely decrease the contribution of annihilation, they have also been used to identify annihilation-specific phenomena, such as excimer formation, that occur during ECL but not during PL.[10]

Scheme 2

$$R + e \rightarrow R^{\bullet -} \quad (5)$$

$$R^{\bullet -} + S_2O_8^{2-} \rightarrow R + SO_4^{2-} + SO_4^{\bullet -} \quad (6)$$

$$R^{\bullet -} + SO_4^{\bullet -} \rightarrow R^* + SO_4^{2-} \quad (7)$$

$$R^* \rightarrow R + h\nu \quad (8)$$

Generally, planar molecules such as 9,10-dimethylanthracene will have a greater probability of forming excimers in both PL and ECL.[11,12] In DPA, however, the phenyl substituents are so bulky that they are rotated out of the anthracene plane by about 68°,[13] and excimer formation is sterically inhibited.[14] Spiro-FPA possesses steric hindrance similar to that of DPA, but each spiro-FPA molecule consists of two redox centers, so the radical ions created at the electrode surface carry 2+ and 2− charges. The charges on the molecule are separated from one another by the spirobifluorene moiety, so we represent the dication as $PA^{\bullet +}\sim X\sim PA^{\bullet +}$ and the dianion as $PA^{\bullet -}\sim X\sim PA^{\bullet -}$. The attraction between the radical di-ions is 4 times greater than that between mono-ions. If this additional attractive force is sufficient to overcome the steric hindrance created by the 9,10 substituents, excimer emission will be visible in the ECL spectrum. Thus, it should be possible to distinguish between mono-ion annihilation and di-ion annihilation.

Scheme 3

$$PA^{\bullet -}\sim X\sim PA^{\bullet -} + PA^{\bullet +}\sim X\sim PA^{\bullet +} \rightarrow \begin{matrix} PA^{\bullet -}\sim X\sim PA^{\bullet -} \\ PA^{\bullet +}\sim X\sim PA^{\bullet +} \end{matrix} \quad (9)$$

$$\begin{matrix} PA^{\bullet -}\sim X\sim PA^{\bullet -} \\ PA^{\bullet +}\sim X\sim PA^{\bullet +} \end{matrix} \rightarrow \begin{matrix} PA^{\bullet -}\sim X\sim (PA)^* \\ PA^{\bullet +}\sim X\sim PA \end{matrix} \quad (10)$$

$$\begin{matrix} PA^{\bullet -}\sim X\sim (PA)^* \\ PA^{\bullet +}\sim X\sim PA \end{matrix} \rightarrow \begin{matrix} PA\sim X\sim PA^{\bullet -} \\ PA^{\bullet +}\sim X\sim PA \end{matrix} \quad (11)$$

$$\begin{matrix} PA^{\bullet -}\sim X\sim PA^{\bullet -} \\ PA^{\bullet +}\sim X\sim PA^{\bullet +} \end{matrix} \rightarrow \begin{matrix} (PA)^*\sim X\sim (PA)^* \\ PA\sim X\sim PA \end{matrix} \quad (12)$$

Scheme 3 shows the pathways for excimer formation and emission. The activated complex is represented by vertically stacked spiro-FPA di-ions, as shown in reaction 9. Since an excimer created by a one-electron transfer between the di-ions should be rapidly quenched by an intramolecular electron transfer from the other redox center, as shown in reactions 10 and 11, excimer emission from these molecules suggests the possibility of a simultaneous, two-electron transfer mechanism (reaction 12).

By varying the electrolyte concentration, we observe a correlation between the effective electrostatic attraction between

(1) (a) Cauquis, G. Basic Concepts. In *Organic Electrochemistry*; Baizer, M., Ed.; Marcel Dekker, Inc.: New York, 1973; pp 43–48. (b) Bard, A.; Faulkner, L. *Electrochemical Methods: Fundamentals and Applications*, 2nd ed.; John Wiley & Sons, Inc.: New York, 2001; pp 108475–476. (c) Zanelo, P. *Inorganic Electrochemistry: Theory, Practice, and Application*; The Royal Society of Chemistry: Cambridge, UK, 2003; pp 99–100..

(2) Jordan, J.; Javick, R. A. *J. Am. Chem. Soc.* **1958**, *80*, 1264.

(3) Elving, P. J.; Leone, J. T. *J. Am. Chem. Soc.* **1957**, *79*, 1546.

(4) Murov, S. L.; Carmichael, I.; Hug, G. L. *Handbook of Photochemistry*, 2nd ed., revised and expanded; Marcel Dekker, Inc.: New York, 1993; p 9.

(5) Itoh, K.; Honda, K.; Sukigara, M. *Electrochim. Acta* **1979**, *24*, 1195.

(6) (a) Phelps, J.; Santhanam, K. S. V.; Bard, A. J. *J. Am. Chem. Soc.* **1967**, *89*, 1752. (b) Sioda, R. E. *J. Phys. Chem.* **1968**, *72*, 2322.

(7) Bard, A. J. *Electrogenerated Chemiluminescence*; Marcel Dekker: New York, 2004; p 5.

(8) Shen, W.-J.; Dodda, R.; Wu, C.-C.; Wu, F.-I.; Liu, T.-H.; Chen, H.-H.; Chen, C. H.; Shu, C.-F. *Chem. Mater.* **2004**, *16*, 930.

(9) For reviews on ECL, see: (a) Richter, M. M. *Chem. Rev* **2004**, *104*, 3003–3036. (b) Knight, A. W.; Greenway, G. M *Analyst* **1994**, *119*, 879–890. (c) Faulkner, L. R.; Bard, A. J. *Electroanalytical Chemistry*; Marcel Dekker: New York, 1977; Vol. 10, p 1. (d) Bard, A. J.; Debad, J. D.; Leland, J. K.; Sigal, G. B.; Wilbur, J. L.; Wohlstadter, J. N. In *Encyclopedia of Analytical Chemistry: Applications, Theory and Instrumentation*; Meyers, R. A., Ed.; John Wiley & Sons: New York, 2000; Vol. *11*, p 9842.

(10) (a) Keszthelyi, C. P.; Bard, A. J. *Chem. Phys. Lett.* **1974**, *24*, 300. (b) Park, S. M.; Paffett, M. T.; Daub, G. H. *J. Am. Chem. Soc.* **1977**, *99*, 5394. (c) Choi, J.-P.; Wong, K.-T.; Chen, Y.-M.; Yu, J.-K.; Chou, P.-T.; Bard, A. J. *J. Phys. Chem. B* **2003**, *107*, 14407.

(11) Werner, T.; Chang, J.; Hercules, D. *J. Am. Chem. Soc.* **1970**, *92*, 763.

(12) Birks, J. B. *Photophysics of Aromatic Molecules*; Wiley-Interscience: New York, 1970; Chapter 7.

(13) Bard, A.; Santhanam, K.; Maloy, J.; Phelps, J.; Wheeler, L. *Discss. Faraday Soc.* **1968**, *45*, 167.

(14) Chandross, E.; Longworth, J.; Visco, R. *J. Am. Chem. Soc.* **1965**, *87*, 3259.

geminate radical ion pairs and the relative excimer emission. Therefore, the ionic strength plays a significant role in overcoming the steric barrier to excimer formation. With these data, we show how a molecule with multiple redox centers might be used to demonstrate simultaneous, two-electron transfer.

Experimental Section

Materials. Spiro-FPA was synthesized as previously reported.[8] Anhydrous MeCN was obtained from Aldrich (St. Louis, MO) and transferred directly into an inert atmosphere drybox (Vacuum Atmospheres Corp., Hawthorne, CA). Anhydrous PhH was obtained from Aldrich and distilled under vacuum to remove an electroactive impurity before transfer into the drybox. The supporting electrolyte, tetra-*n*-butylammonium perchlorate (TBAP), was obtained from Fluka and used as received. All solutions were prepared inside of the drybox and sealed in airtight cells for measurements outside of the drybox. Tetra-*n*-butylammonium peroxydisulfate ($TBA_2S_2O_8$) was prepared from tetrabutylammonium hydrogen sulfate and $K_2S_2O_8$ according to a literature procedure.[15]

Characterization. Cyclic voltammograms (CVs) were obtained on a CH Instruments 660 electrochemical workstation (Austin, TX). The working electrode (WE) was a 0.5 mm Pt disk, inlaid in glass. For ECL experiments, a 1.5 mm inlaid Pt disk WE was bent at 90° so it faced the detector. The WE in each case was polished on a felt pad with 0.3 μm alumina (Buehler Ltd., Lake Bluff, IL) and then sonicated in water followed by ethanol for 1 min each before being rinsed with acetone and transferred into the drybox. The counter electrode was a Pt wire. An Ag wire was used as a quasi-reference electrode and calibrated with ferrocene (0.342 V vs SCE).[16] All solutions for electrochemical experiments contained 0.5 mM spiro-FPA and 0.1 M TBAP in 3:1 PhH/MeCN. Co-reactant ECL solutions also contained 10 mM $TBA_2S_2O_8$. Solutions were prepared in a glass cell inside the drybox. The cells were closed with a Teflon cap fitted with a rubber O-ring to form an airtight seal so measurements could be made outside the box. Stainless steel rods were driven through the cap to form the electrode connections several centimeters above the solution level.

Absorbance spectra were collected on a DU 640 spectrophotometer (Beckman, Fullerton, CA) using a 56 μM solution of spiro-FPA in 3:1 PhH/MeCN in a 1 cm quartz cell and a 52 μM solution of DPA in the same solvent. PL spectra of solutions of 560 nM spiro-FPA and 520 nM DPA, both in 3:1 PhH/MeCN, were obtained using a QuantaMaster spectrofluorimeter (Photon Technology International, Birmingham, NJ) with a 2 nm band-pass at the excitation and emission slits.

ECL spectra were obtained by pulsing the electrode potential 80 mV beyond the reduction and oxidation peak potentials (i.e., between $E_{p,ox} + 80$ mV and $E_{p,red} - 80$ mV), using an Eco Chemie (The Netherlands) Autolab potentiostat. Co-reactant ECL spectra were generated by pulsing between 0 V and $E_{p,red} - 80$ mV. ECL spectra were collected using a Princeton Instruments (Trenton, NJ) charge-coupled device (CCD) camera cooled to −100 °C with an Acton SpectraPro-150 monochromator (Acton, MA). The CCD monochromator was calibrated with a Hg lamp after a spectrum was obtained.

Simulations. Two-dimensional digital simulations of the electrochemical processes were performed using the DigiElch software package.[17] The double-layer capacitance of 17.1 nF and the uncompensated resistance of 6155Ω were extracted from the current transient for a potential step in a region where only nonfaradaic current flowed. The electrode area used in the simulations was determined from a Cottrell plot obtained in 1 mM ferrocene in MeCN, taking the diffusion coefficient as 2.4×10^{-5} cm^2/s.[18] All electrochemical processes were treated as diffusion controlled and assigned heterogeneous electron-transfer rate constants of $k^\circ = 10$ cm/s. The diffusion coefficient, D, and the redox potentials were adjusted until the best fit was obtained between experiment and simulation.

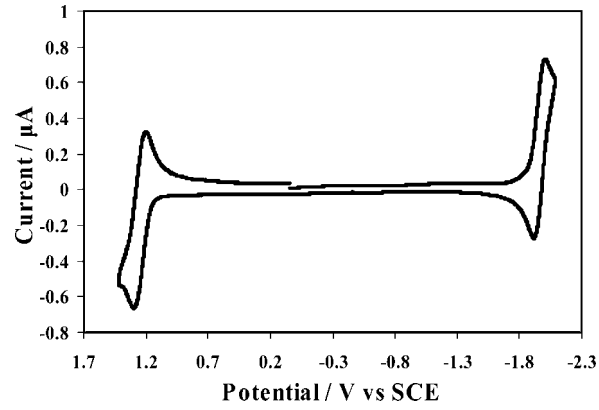

Figure 2. Cyclic voltammogram of 0.5 mM spiro-FPA in 3:1 benzene/acetonitrile. Scan rate = 200 mV/s.

ECL simulations of the di-ion annihilation were performed using COMSOL Multiphysics 3.3 (COMSOL, Inc.). The diffusing species were confined to a 2.4 mm 1-D cell consisting of 118 mesh elements. The mesh size was 10 nm at the electrode surface and expanded by factors of 1.2 with increasing distance from the electrode. The Butler–Volmer equation was used as the electrode boundary condition, and spiro-FPA was assigned heterogeneous electron-transfer rate constants $k^\circ = 10$ cm/s for all electrode reactions. The analyte was allowed two separate, one-electron reductions and oxidations at the electrode. The electrode potential was pulsed between −2.13 and 1.30 V vs SCE at 10 Hz by using Heaviside functions to switch on one potential while the other was off. All data were taken from the fourth potential pulse (a reduction).

All annihilation (homogeneous electron transfer) reactions between anions and cations, as well as excited-state quenching reactions by radical ion species, were assigned a rate constant, k_{ann}, of 2×10^8 M^{-1} s^{-1}.[19] Monomer excited states were quenched by electron transfer from any spiro-FPA ion in solution, using $k_{rq} = 2 \times 10^8$ M^{-1} s^{-1}. The rate constant for emission from the excited state was chosen as $k_{em} = 1.4 \times 10^8$ s^{-1}.[20]

Results and Discussion

Electrochemistry. Cyclic voltammetry was used to assess the stability of the reduced and oxidized spiro-FPA species. A CV showing both oxidation and reduction of spiro-FPA is presented in Figure 2. Comparison of digital simulations and experimental CVs of the oxidation are shown in Figure 3 and corresponding reductions with similar fits in Figure S1 (Supporting Information). The CV simulation mechanism assigned two reversible, one-electron processes to both oxidation and reduction, with a ΔE° between the two waves of 50 mV on the reduction side and 60 mV on the oxidation side, and $D = 8.5 \times 10^{-6}$ cm^2/s. Thus, $E^\circ_{1,red} = -2.02$, $E^\circ_{2,red} = -2.07$ V vs SCE and $E^\circ_{1,ox} = 1.14$, $E^\circ_{2,ox} = 1.20$ V vs SCE.

(15) Park, M. Y.; Yang, S. G.; Jadhav, V.; Kin, Y. H. *Tetrahedron Lett.* **2004**, *45*, 4887.
(16) Sahami, S.; Weaver, M. *J. Electroanal. Chem.* **1981**, *122*, 155.
(17) (a) Rudolph, M. *J. Electroanal. Chem.* **2003**, *543*, 23. (b) Ruldolf, M *J. Electroanal. Chem.* **2004**, *571*, 289. (c) Rudolph, M. *J. Electroanal. Chem.* **2003**, *558*, 171. (d) Rudolph, M. *J. Comput. Chem.* **2005**, *26*, 619. (e) Rudolph, M. *J. Comput. Chem.* **2005**, *26*, 233. (f) Rudolph, M. *J. Comput. Chem.* **2005**, *26*, 1193.
(18) Kadish, K. M.; Ding, J. Q.; Malinski, T. *Anal. Chem.* **1984**, *56*, 1741.
(19) Collinson, M.; Wightman, M.; Pastore, P *J. Phys. Chem.* **1994**, *98*, 11942. The reported value, 2×10^{10} M^{-1} s^{-1}, resulted in negative concentrations, but 10^8 was deemed fast enough to adequately represent the data on the time scale of this experiment. .
(20) Boens, N.; et al. *Anal. Chem.* **2007**, *79*, 2137.

$$\mathrm{PA{\sim}X{\sim}PA} + \mathrm{e} \rightarrow \mathrm{PA{\sim}X{\sim}PA^{\bullet -}} \qquad E^{\circ}_{1,\mathrm{red}} \qquad (13)$$

$$\mathrm{PA{\sim}X{\sim}PA^{\bullet -}} + \mathrm{e} \rightarrow \mathrm{PA{\sim}X{\sim}PA^{\bullet 2-}} \qquad E^{\circ}_{2,\mathrm{red}} \qquad (14)$$

$$\mathrm{PA{\sim}X{\sim}PA} - \mathrm{e} \rightarrow \mathrm{PA{\sim}X{\sim}PA^{\bullet +}} \qquad E^{\circ}_{1,\mathrm{ox}} \qquad (15)$$

$$\mathrm{PA{\sim}X{\sim}PA^{\bullet +}} - \mathrm{e} \rightarrow \mathrm{PA{\sim}X{\sim}PA^{\bullet 2+}} \qquad E^{\circ}_{2,\mathrm{ox}} \qquad (16)$$

The plots in Figures 3 and S1 indicate good fits between experimental and simulated CVs performed at scan rates (ν) from 50 mV/s to 10 V/s. The small deviations that occur in the reduction simulations at high scan rates are likely due to either uncompensated resistance that was underestimated in the simulation or slow heterogeneous electron-transfer kinetics on the reduction.

For DPA, $E^{\circ}_{\mathrm{red}} = -2.06$ V vs SCE and $E^{\circ}_{\mathrm{ox}} = 1.15$ V vs SCE. Since $E^{\circ}_{\text{spiro-FPA}} \approx E^{\circ}_{\mathrm{DPA}}$ for both oxidation and reduction, both redox centers of spiro-FPA are similar to an isolated DPA molecule; however, since $E^{\circ}_2 - E^{\circ}_1 > 35.6$ mV (the expected statistical value for no interaction), some small interaction may exist between the two redox centers of spiro-FPA.[21]

The potentials of the DPA second oxidation[22] and reduction[23] waves were compared to those of the corresponding spiro-FPA waves to assess whether the conjugation through the fluorene moiety or the presence of an additional, charged PA unit would affect the potentials of additional waves. Scanning the potential negative beyond the first reduction revealed no additional waves before the solvent window was reached. Since DPA gave the same result, the absence of additional reduction waves is

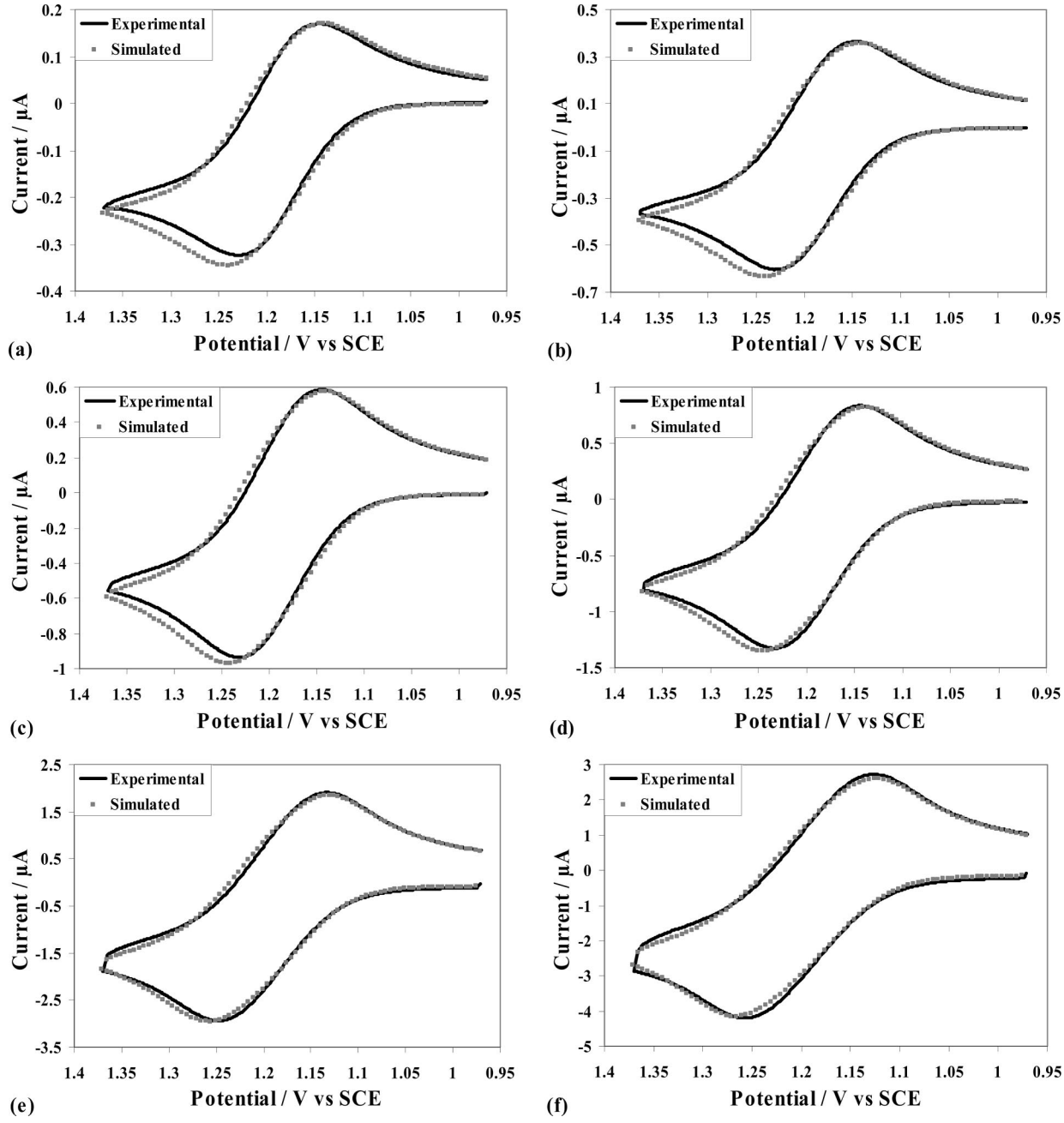

Figure 3. Simulation of 0.5 mM spiro-FPA oxidation at (a) 50 mV/s, (b) 200 mV/s, (c) 500 mV/s, (d) 1 V/s, (e) 5 V/s, and (f) 10 V/s. Simulation mechanism is two, one-electron oxidations with $D = 8.5 \times 10^{-6}$ cm^2/s, $E^{\circ}_{1,\mathrm{ox}} = 1.14$ V vs SCE, $E^{\circ}_{2,\mathrm{ox}} = 1.20$ V vs SCE, $k^{\circ} = 10^4$ cm/s, $\alpha = 0.5$, $R_u = 6155\ \Omega$, and $C_d = 17.1$ nF.

Table 1. Spectroscopic Data for Spiro-FPA and DPA

λ_{abs}/nm	ϵ/M^{-1} s^{-1}	λ_{PL}/nm	Φ_{PL}	Φ_{ECL}
		DPA		
356	8 500	420	0.91	0.014
374	13 800			
395	13 100			
		Spiro-FPA		
358	16 300	434	0.74	0.0042
377	25 700			
397	24 800			

attributed to adventitious water narrowing the solvent window. Scanning the potential positive beyond the first oxidation wave revealed a chemically irreversible second oxidation with peak potential $E_p = 1.58$ V vs SCE. DPA gives a second oxidation wave at $E_p = 1.59$ V vs SCE. The similarity between second oxidation potentials emphasizes the lack of communication between PA centers.

Spectroscopy. The spectroscopic characteristics of spiro-FPA were compared to those of DPA to determine the effects of the bifluorene linking group on the PA moieties. The data are summarized in Table 1. The absorbance maxima, $\lambda_{max,abs}$, for all three major peaks of both molecules are within 3 nm of each other, as shown in Figure 4. The extinction coefficients, ϵ, for each of the major vibronic bands of spiro-FPA are approximately twice as large as their DPA counterparts. Thus, spiro-FPA has twice the number of effective chromophores in a solution as the same concentration of DPA. The short wavelength absorbance of spiro-FPA is attributed to absorption by the bifluorene moiety.

Photoluminescence spectra were generated by exciting DPA at 374 nm and spiro-FPA at 377 nm. The DPA emission maximum occurs at 420 nm, and the spiro-FPA emission maximum occurs at 434 nm, as shown in Figure 5. Since $\lambda_{max,abs}$ is the same for both molecules, the 15 nm bathochromic shift suggests that more structural rearrangement occurs in the excited state of spiro-FPA than in DPA. This greater flexibility may also increase internal conversion and lower the quantum yield for PL, as spiro-FPA exhibits a Φ_{PL} of 0.76.

ECL Experiments. The spiro-FPA ECL spectrum, generated by pulsing between the first oxidation and reduction peaks, appears to be bathochromically shifted by 15 nm from the PL spectrum, giving a λ_{max} of 450 nm (Figure 6). However, since the DPA spectrum shows the same shift, this is attributed to the larger self-absorption of the emission by the 0.5 mM ECL samples compared to those for PL. A more significant difference between the ECL and PL spectra, however, is the long-wavelength ECL emission that extends to 720 nm. Long-wavelength ECL not observed in the PL typically results from either a side product of the electrochemistry[24] or the formation of excimers. The broad, structureless nature of the long-wavelength emission is consistent with excimer formation. In another experiment shown in Figure 6, ECL was obtained by reduction in the presence of $TBA_2S_2O_8$ as a co-reactant. In this case, the long wavelength emission was greatly diminished, also consistent with formation of excimers.

However, one would expect the large steric hindrance to π-stacking between two spiro-FPA molecules to make excimer formation improbable, especially since the steric hindrance of the similarly structured DPA prevents excimer formation in both PL and ECL. However, unlike DPA electrochemistry, spiro-FPA oxidation and reduction both generate di-ions. According to the Coulomb equation, electrostatic attraction between 2+ and 2− charges is 4 times greater than that between their mono-ion counterparts, which may be sufficient to overcome the steric barrier to excimer formation. However, within electron-transfer distance, the 2+ and 2− charges can no longer be treated as

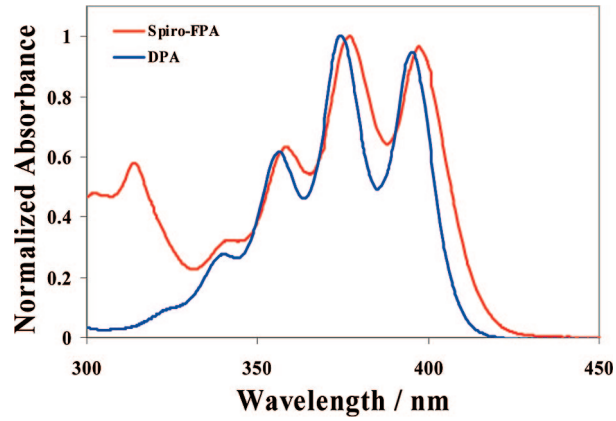

Figure 4. Absorbance spectra of solutions of 52 μM spiro-FPA and 56 μM DPA in 3:1 PhH/MeCN.

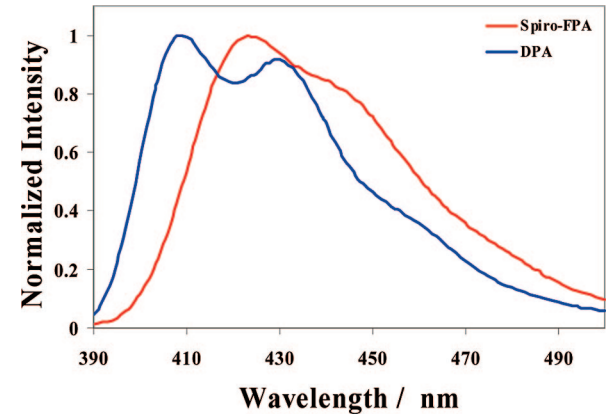

Figure 5. Fluorescence spectra of solutions of 0.52 μM spiro-FPA and 0.56 μM DPA in 3:1 PhH/MeCN.

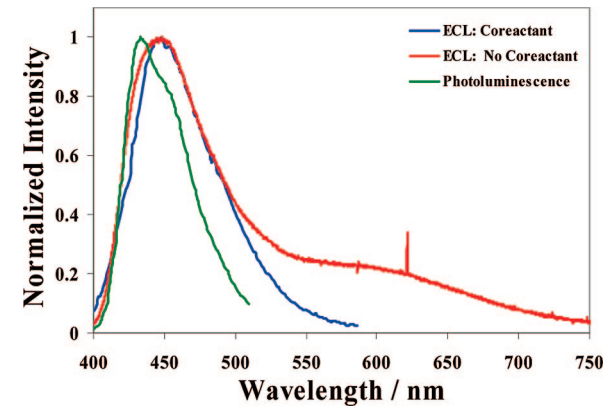

Figure 6. Photoluminescence spectrum of 0.52 μM spiro-FPA and ECL spectra of 0.5 mM spiro-FPA in 3:1 PhH/MeCN. ECL spectra were taken with and without 10 mM $S_2O_8^{2-}$ co-reactant.

(21) Bard, A. J.; Faulkner, L. R. *Electrochemistry: Fundamentals and Applications*; John Wiley & Sons: New York, 2001; pp 245–246.
(22) Sioda, R. *J. Phys. Chem.* **1968**, *72*, 2322.
(23) Santhanam, K. S. V.; Bard, A. J. *J. Am. Chem. Soc.* **1966**, *88*, 2669.
(24) Faulkner, L. R.; Bard, A. J. *J. Am. Chem. Soc.* **1968**, *90*, 6284.

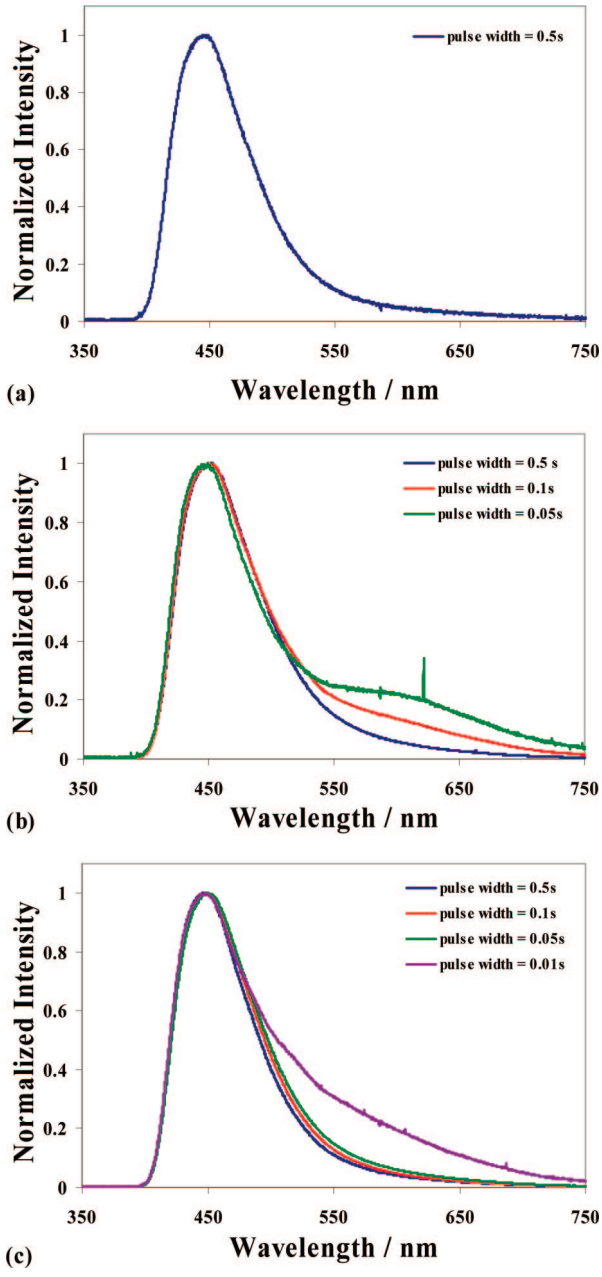

Figure 7. ECL spectra of 0.5 mM spiro-FPA obtained at various pulse widths using the following electrolyte concentrations: (a) 0.01 M TBAP, (b) 0.05 M TBAP, and (c) 0.14 M TBAP.

point charges, and the electrostatic attraction between the molecules is actually only increased by a factor of 2.

If electrostatic attraction plays a role in excimer formation, a study of the ECL spectra at different supporting electrolyte concentrations should be useful. With low electrolyte concentration, the radical ions are less shielded from one another, so the stronger attraction between di-ions should become more apparent, yielding higher relative excimer emission, while at higher concentrations there should be significant shielding. However, at low electrolyte concentrations, the *RC* time constant becomes significant; this limits the pulse widths that can be used to obtain the ECL spectra at low electrolyte concentrations. Figure 7 shows ECL spectra at different concentrations of TBAP and pulse widths. In 0.01 M TBAP, the *RC* constant prevented the use of pulse widths shorter than 0.5 s, and no excimer emission was observed at any TBAP concentration at a pulse width of 0.5 s. However, one can compare the results in 0.05 and 0.14 M TBAP at shorter pulse widths. These are consistent with the electrostatic attraction hypothesis for experiments performed with the same pulse width. In 0.14 M TBAP, excimer emission was observed only at a pulse width of 0.01 s, while in 0.05 M TBAP, it was observed at 0.05 and 0.1 s.

Table 2. Relative Excimer Formation from 0.5 mM Spiro-FPA in 3:1 PhH/MeCN at Various Pulse Widths and Concentrations of Electrolyte, TBAP[a]

solution	pulse width/s	excimer fraction
0.01 M TBAP	0.5	0.06
0.05 M TBAP	0.5	0.09
	0.1	0.16
	0.05	0.23
0.14 M TBAP	0.5	0.06
	0.1	0.08
	0.05	0.09
	0.01	0.25
10 mM S_2O_8 and 0.1 M TBAP	0.1	0.004

[a] Excimer fraction is defined as the intensity at 575 nm normalized by the peak intensity (450 nm).

Scheme 4

$$A^{2-} + A^{\bullet+} \rightarrow A^{\bullet-} + A^* \quad (17)$$

$$A^{2-} + A \rightarrow 2A^{\bullet-} \quad (18)$$

In Table 2, excimer formation is calculated as the background-subtracted intensity at 575 nm divided by the background-subtracted peak intensity (450 nm). Values below about 0.05 indicate essentially no excimer formation, whereas values around 0.2 were the largest observed in these experiments. The data show greater relative excimer formation in samples with shorter pulse widths and lower electrolyte concentrations. Note that the pulse width dependence is also inconsistent with long-wavelength emission from a reaction product of the reduced or oxidized form, since emission from a product would be favored at longer pulse widths. Moreover, the electrochemistry shows no sign of follow-up reactions, even at slow scan rates.

ECL Simulations. To understand the pulse width dependence of the excimer formation, the concentration profiles of the excited monomer and excimer were examined using simulations of a potential pulse (Figure S2). The simulation assumed electrode reactions, (13) through (16), followed by various homogeneous electron-transfer reactions, such as (9) through (12) that lead to excited states, followed by emission and quenching of the excited states by reactions with radical ions. Because of the complexity of the mechanism, arbitrary, but experimentally reasonable, rate constants were selected in the simulation (see Experimental Section). The results should be qualitatively meaningful, however. Note that excited states can also form from the mono-ions that are formed when the di-ions diffusing from the electrode undergo comproportionation reactions with incoming parent ions (e.g., Scheme 4).

The results of the simulation are concentrations of all species as a function of distance from the electrode and time. A plot of the peak concentration of the monomeric excited state and excimer versus time (Figure 8) shows a more rapid decrease in excimer concentration than excited monomer concentration. This is probably due to the greater number of scavenging reactions available for di-ions than for mono-ions (Scheme 4). For instance, a di-ion can react with a mono-ion to create either a monomer excited state and a mono-ion (reaction 17) or an excited state with a radical ion, which would quench, as in

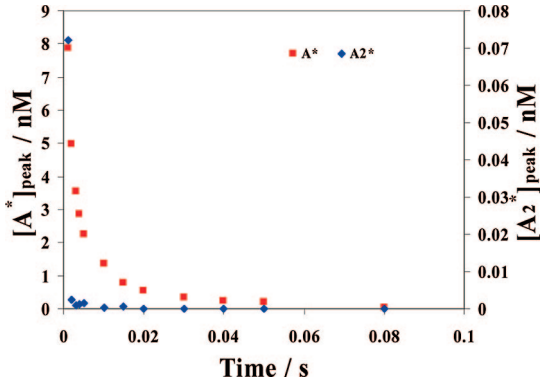

Figure 8. Simulated decay of spiro-FPA excimer and excited monomer concentration with time following an ECL potential pulse.

reaction 11. In the latter case, the simulation model used the ground-state mono-ion as the direct product of the di-ion/mono-ion annihilation, excluding the excited state with a radical ion. Also, a di-ion can comproportionate with neutral spiro-FPA to create two mono-ions, as in reaction 18. The equilibrium constant for comproportionation processes, calculated from experimentally determined $E°$ values, is 7 for the dianion and 10 for the dication. Assuming that the difference between K_{eq} values is within experimental error, $K_{eq} = 8.5$ was assigned to both dianion and dication comproportionation and maintained by choosing $k_{f,com} = 2.000 \times 10^8\ M^{-1}\ s^{-1}$ and $k_{b,com} = 0.235 \times 10^8\ M^{-1}\ s^{-1}$. As observed in reactions 10 and 11, di-ion annihilation may result in only a one-electron transfer, which would yield two ground-state mono-ions.

Experiments that use shorter pulse widths yield a larger fraction of excimer emission because they occur in the time regime before the additional decomposition reactions prevent significant excimer formation. While the simulated decay rate is in general agreement with the experimental results, given the complexity of the reaction scheme, this cannot be taken as confirmation of the proposed mechanism. For example, the effects of TBAP concentration and the mutual attraction between di-ions are not considered in this simulation.

We propose here a concerted or essentially simultaneous electron-transfer reaction to produce the excimer state. This is largely based on the assumption that any stepwise electron transfer would produce an intermediate that would rapidly be intramolecularly quenched by the radical ion component before it had a chance to radiate. Such a two-electron transfer would ordinarily not be favored, but in this case the large free energy difference would promote a reaction that should occur at a very high rate, approaching diffusion control. It might produce a higher (e.g., doubly) excited state, but this would probably relax rapidly before emission to yield the monomeric or dimeric excited state.

Conclusions

Spiro-FPA is comprised of two PA moieties, both of which undergo electrochemical processes at approximately the same potentials, indicating minimal interaction between them. Because there are two redox centers, di-ions are created during each potential pulse of an ECL experiment. The electrolyte concentration dependence of the long wavelength emission observed during annihilation ECL (but not in PL) demonstrates the importance of high electrostatic charge to overcoming the steric hindrance to excimer formation. Solutions with lower electrolyte concentrations exhibit a larger fraction of excimer emission, because the greater electrostatic attraction between di-ions relative to mono-ions is more apparent in the absence of electrostatic shielding. Additionally, shorter pulse widths result in still higher relative excimer emission because the short time scales decrease the contribution from reactions that consume the di-ions before their annihilation. Since the annihilation occurs between di-ions, a single electron transfer to form an excimer should be quenched by intramolecular transfer of the other electron prior to emission. Therefore, the presence of excimer emission in spiro-FPA is most reasonably explained by a simultaneous two-electron transfer.

Acknowledgment. We thank BioVeris Corp., the Robert A. Welch Foundation, and the National Science Foundation (CHE-0451494) for support of this research.

Supporting Information Available: CVs and simulations of spiro-FPA reduction (Figure S1), simulations of the excited monomer and excimer concentration profiles (Figure S2), and complete ref 20. This information is available free of charge via the Internet at http://pubs.acs.org.

JA8000858